Tectonics

RESEARCH ARTICLE
10.1029/2022TC007602

3D Geophysical and Geological Modeling of the South Orkney Microcontinent (Antarctica): Tectonic Implications for the Scotia Arc Development

Cecilia Morales-Ocaña[1], Fernando Bohoyo[2], Carlota Escutia[1], Carlos Marín-Lechado[2], Carmen Rey-Moral[2], María Druet[2], Jesús Galindo-Zaldívar[1,3], and Adolfo Maestro[2]

[1]Instituto Andaluz de Ciencias de la Tierra (IACT), CSIC-UGR, Granada, Spain, [2]Instituto Geológico y Minero de España (IGME-CSIC), Madrid, Spain, [3]Departamento de Geodinámica, Facultad de Ciencias, Universidad de Granada, Granada, Spain

Key Points:

- 3D modeling outlines the geometry of the sedimentary basins, intrusive igneous body and Moho in the South Orkney Microcontinent
- Modeled deformation is coherent with strong extension east of the Microcontinent during the early stages of the Scotia Arc formation
- Extension migrated westwards causing the opening and oceanization of the Powell Basin

Correspondence to:
C. Morales-Ocaña,
cecilia.morales@csic.es

Citation:
Morales-Ocaña, C., Bohoyo, F., Escutia, C., Marín-Lechado, C., Rey-Moral, C., Druet, M., et al. (2023). 3D geophysical and geological modeling of the South Orkney Microcontinent (Antarctica): Tectonic implications for the Scotia Arc development. *Tectonics*, *42*, e2022TC007602. https://doi.org/10.1029/2022TC007602

Received 20 SEP 2022
Accepted 11 MAR 2023

Abstract The opening of the Scotia Arc resulted in the final breakup of the land bridge between South America and the Antarctic Peninsula. The South Orkney Microcontinent (SOM) constituted part of this former connection and it is now the largest continental block in the Southern Scotia Arc. We present the first 3D model of the SOM that, given its strategic position and characteristics, allows us to advance the knowledge of the tectonic processes involved in the development of the Scotia Arc. Due to the scarcity of reliable geological data, the initial approximation of the deep structure of the SOM was supported by the calculation of three main geological boundaries from geophysical data: the acoustic basement, the boundary of the magnetic anomaly source and the Moho depth. The 3D model was built, refined and validated by forward modeling and joint inversion of gravity and magnetic data. We have accurately defined the geometry of the sedimentary cover, determined the geometry of the intrusive igneous body causing the Pacific Margin Anomaly (PMA) and mapped the heterogeneity of the crustal thickness. These structural features show a clear relationship to each other and are consistent with an important E-W extension to the east of the SOM during early stages of the Scotia Arc formation, prior to the opening of the Powell Basin.

1. Introduction

The origin of the Scotia Arc lies in the early stages of the fragmentation of the supercontinent Gondwana during the late Mesozoic (Dalziel et al., 2013), which culminated in the separation between South America and the Antarctic Peninsula, thus opening the Drake Passage (P. F. Barker & Burrell, 1977). The South Orkney Microcontinent (SOM) is the largest continental block in the South Scotia Arc, located between the Scotia and the Antarctic plates. Previous work has postulated the SOM to be the final continental link between the Antarctic Peninsula and South America (Lawver et al., 1985). Paleogeographic reconstructions place the SOM adjacent to the eastern Antarctic Peninsula and close to South America before the opening of the Scotia Arc and the Drake Passage (Dalziel et al., 2013; Eagles & Jokat, 2014; Livermore et al., 2005; van de Lagemaat et al., 2021). However, many uncertainties remain as to when and how the dispersion of the continental blocks occurred in the Scotia Arc (Riley et al., 2022). These uncertainties in turn, prevent accurate paleoceanographic reconstructions of the earliest connection between the Pacific and Atlantic Oceans and hinder confident understanding of the implications for global ocean circulation and climate.

Previous works carried out in the study area, although scarce, have defined the main structural characteristics of the SOM: (a) The geometry of the sedimentary basins of the SOM from geophysical data facilitated the recognition of two structural trends (i.e., a younger N-S overlying an older E-W trend) (King & Barker, 1988). (b) The continuity of a large amplitude magnetic anomaly belt—the Pacific Margin Anomaly (PMA)—along the dispersed continental fragments of the Scotia Arc, allowed the reconstruction of the former connection between the SOM and the Antarctic Peninsula (P.F. Barker & Griffiths, 1972; Eagles & Livermore, 2002; Garrett et al., 1986/87; Martos et al., 2014). (c) The crustal thickness below the SOM has been described as unusually thin as an expression of the extensional tectonic regime it has undergone (King & Barker, 1988). So far, those works have characterized these features separately resulting in a limited understanding of the origin and evolution of the SOM.

10.1029/2022TC007602

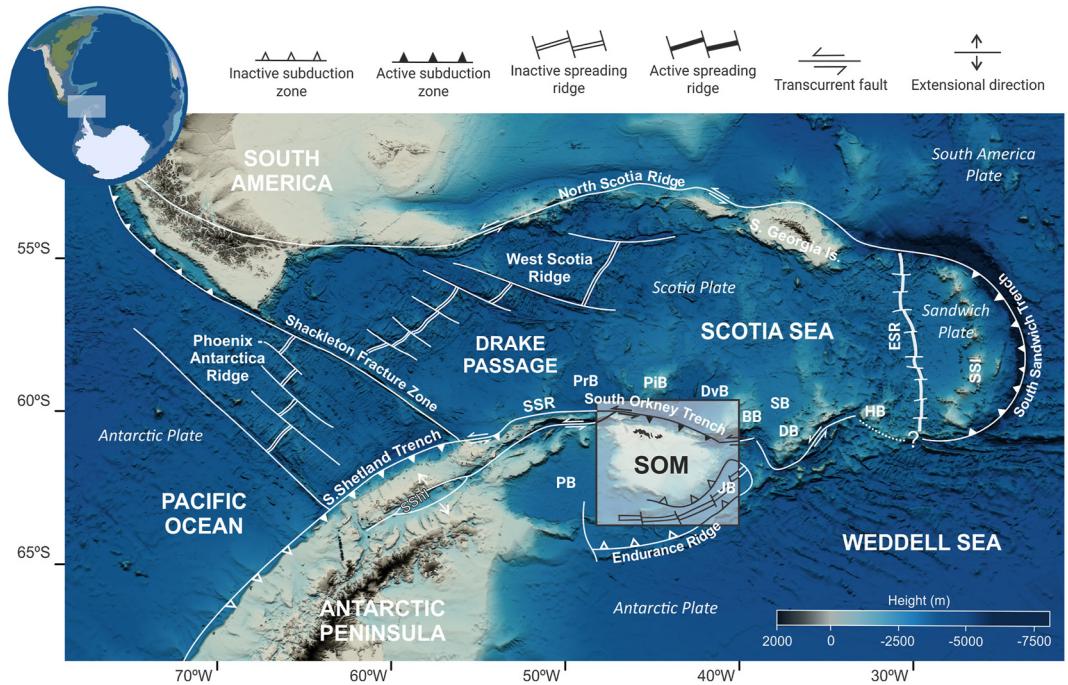

Figure 1. Tectonic setting of the Scotia Arc. Bathymetry from GEBCO 2020. BB, Bruce Bank; DB, Discovery Bank; DvB, Dove Basin; ESR, East Scotia Ridge; HB, Herdman Bank; JB, Jane Basin; PB, Powell Basin; PiB, Pirie Bank; PrB, Protector Basin; SB, Scan Basin; SOM, South Orkney Microcontinent; SShI, South Shetland Islands; SSI, South Sandwich Islands; SSR, South Scotia Ridge.

The aim of this study is to improve the resolution of the aforementioned structural features of the SOM and to interrelate their geometries to reveal new insights into the tectonic processes operating during the different stages of the Scotia Arc formation, from the Mesozoic to the present. 3D modeling represents a powerful tool that facilitates the integration of different geological and geophysical datasets (Calcagno et al., 2008; Mallet, 2002; Wu et al., 2005) and allows to characterize large geological structures in data-poor regions such as Antarctica. We present the first 3D geophysical and geological model of the SOM and its surroundings by gravity and magnetic forward modeling and joint inversion. The model has been constrained by three main geological boundaries: the acoustic basement inferred from multichannel seismic reflection (MCS) profiles, the PMA source boundary and the Moho. The model resolves the complex geological structure of the SOM, including refinement of the geometry of the sedimentary basins, the magnetic source of the PMA and the variation of the crustal thickness, providing new insights into the tectonic evolution of the SOM.

2. Geological Setting

The SOM is located in the southern branch of the Scotia Arc and is the largest continental block in the area (nearly 70,000 km^2). At present, the SOM is integrated in the Antarctic plate and its northern margin constitutes an active segment of the boundary between the Scotia and Antarctic plates (Figure 1).

The tectonic evolution of the SOM since the Mesozoic has been inferred by the analysis of lineaments and brittle structures measured in rock outcrops in the South Orkney Islands, the only exposed part of the microcontinent (Maestro et al., 2013; Trouw et al., 1997). Trouw et al. (1997) established up to five phases of deformation. In the early Mesozoic (phases 1–3), the SOM was still attached to the Antarctic Peninsula and the deformation was north-south trending as a response to the subduction of the former Phoenix plate beneath the Gondwana margin (P. F. Barker et al., 1991). During late Jurassic (Phase 4), the opening of the Rocas Verdes Basin (154 Ma) produced an important N-S crustal extension that has been related to the first stages of the Gondwanaland breakup (P. F. Barker et al., 1991). Simultaneously with the Rocas Verdes Basin opening, the Antarctic Peninsula started a rotation relative to East Antarctica. There is no consensus on the sense of rotation, since for some authors it is clockwise and for others counterclockwise (P. F. Barker & Dalziel, 1983; Dalziel, 1984; Eagles &

10.1029/2022TC007602

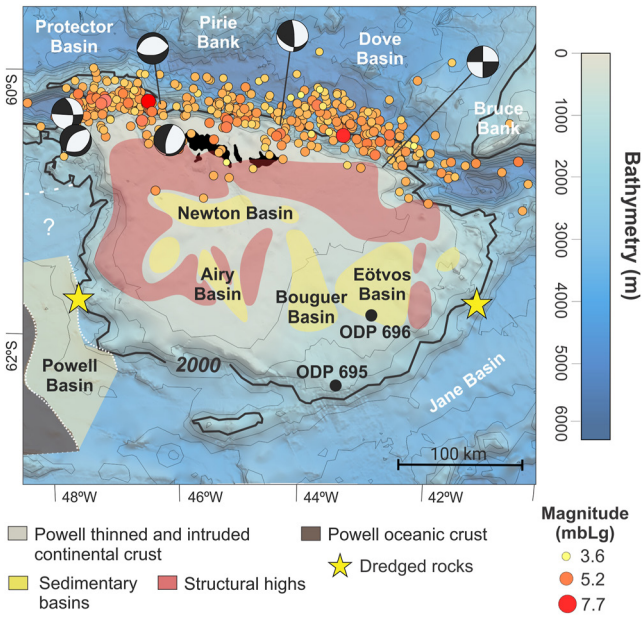

Figure 2. Geological setting of the SOM. Historical seismicity was extracted from the USGS earthquake catalog. Earthquake focal mechanisms after Bohoyo et al. (2007). Position of the sedimentary basins and structural basement highs after Busetti et al. (2000). Powell Basin crustal zones were differentiated in Catalán et al. (2020). Location of the Ocean Drilling Program (ODP) Sites 696 and 695 is also pointed. The location of dredged rocks around the SOM by Barber et al. (1991) is shown with stars.

Eisermann, 2020; van de Lagemaat et al., 2021). The Cenozoic history of the SOM produced a phase of brittle faults of horizontal extension (Phase 5) that has been related with opening of the Powell Basin and the development of the Scotia Arc (Trouw et al., 1997). The opening of the Scotia Arc after 50 Ma and consequently, the opening of the Drake Passage, caused the drift of the different continental blocks, including the SOM (Livermore et al., 2007). The current location of the SOM with respect to the Antarctic Peninsula is the result of the seafloor spreading in Powell Basin, dated between 29 and 21 Ma according to Eagles and Livermore (2002) and between 38 and 29 Ma according to Schreider et al. (2022). Garret et al. (1986/87) proposed a 30° counterclockwise rotation to reconstruct the position of the SOM to when it was attached to the Antarctic Peninsula. Another approach to the reconstruction of the former connection between the SOM and the Antarctic Peninsula was performed by Eagles and Livermore (2002) by applying palinspastic adjustments to the shape of the SOM guided by the gravity signals of the Newton, Airy, Bouguer, and Eötvös Basins.

As a consequence of the tectonic evolution in the area, the SOM presents four margins with distinctive morphologies, sediment distributions and different crustal structures (King & Barker, 1988). The northern margin of the SOM corresponds with a curved segment of the plate boundary between the Antarctic and the Scotia plates. Today, this plate boundary is a zone of sinistral transpression (Bohoyo et al., 2007; Civile et al., 2012), which concentrates the current seismic activity in the area (Figure 2). The western margin of the SOM represents a passive margin connected to the oceanic Powell Basin. Catalán et al. (2020) identified the ocean-continent boundary between Powell Basin and SOM describing a transition zone with extended and intruded continental crust between them (Figure 2). The southern and eastern margins are bounded by the oceanic Jane Basin. Seafloor magnetic anomalies indicates that the subduction of the Weddell Sea spreading center beneath the southeastern SOM could have caused the development of the Jane back-arc Basin between 17.6 and 14.4 Ma, after the end of the subduction of the Weddell Sea, tentatively dated at 20 Ma (Bohoyo et al., 2002).

The knowledge of the deep structure of the SOM is still limited. As a first approach to the deep crustal structure, Harrington et al. (1972) performed a N-S seismic refraction profile west of the South Orkney Islands with results limited to the upper layers. The considerable extension undergone by the SOM resulted in an unusually thin crust (King & Barker, 1988). This major extension is evidenced by the presence of NNW-SSE trending normal faults in the southern portion of the SOM that bound the basins located in the area (King & Barker, 1988). Different authors have modeled the crustal thickness: King and Barker (1988) infer 21 km, Kavoun and Vinnikovskaya (1994) between 14 and 26 km, and Busetti et al. (2000) model around 25 km. King and Barker (1988) computed simple isostatic gravity models across the SOM, resulting in most of the SOM considered to be in isostatic equilibrium except the northern margin. The positive isostatic anomaly in the northern SOM reflects an uplift of the area, most likely related to an active strike-slip movement along the northern margin (King & Barker, 1988). In terms of crustal composition, outcrops in South Orkney Islands indicate that the upper continental crust consists mainly of low-grade metamorphic rocks of Paleozoic to Cretaceous age, intruded by bodies of igneous rocks of Cretaceous age (Dalziel, 1984; King & Barker, 1988; Maestro et al., 2013; Rodriguez-Fernandez et al., 1997). Barber et al. (1991) dredged rock from around Powell Basin and the margins of the SOM and differentiated between two groups of samples. The first group, from the east and west margins of the SOM, was described as hydrothermally altered subalkaline basalts, radiometrically dated with ages between 70 and 85 Ma (stars in Figure 2). The second group corresponds to samples from the western margin of the Powell Basin, which include alkali basalts with ages between 47.7 and 49 Ma and Pliocene/Recent.

Throughout the Antarctic Peninsula, long wavelength, high-intensity magnetic anomalies have been described as the Pacific Margin Anomaly (PMA) or the West Coast Magnetic Anomaly (WCMA) (Garrett, 1990; Renner et al., 1982). Subsequent studies have shown the continuity of this belt in multiple continental fragments - including the SOM - which allows the reconstruction of the continental blocks position in the late Mesozoic

(Martos et al., 2014). The source of this anomaly is likely the presence of linear batholiths of basic-intermediate composition, probably gabbro (Garrett et al., 1986/87), produced by the subduction of the Pacific margin below the Gondwana margin (Garrett & Storey, 1987; King & Barker, 1988; Suriñach et al., 1997). Large intrusive bodies with varying magnetic susceptibilities and thicknesses have been modeled to explain the PMA along the Antarctic Peninsula and the SOM. They are considered to have a maximum thickness between 11 km (Garrett et al., 1986/87, Martos et al., 2014) and 20 km (Harrington et al., 1972). Maximum magnetic susceptibilities used for modeling also vary in a wide range: from 0.006 to 0.8530 SI (Harrington et al., 1972; Martos et al., 2014). Below the SOM, it has been proposed that the source of the magnetic anomaly may have been alternative caused by intrusive bodies resulting from the subduction of the Weddell Sea beneath the microcontinent (Bohoyo et al., 2002).

The sedimentary basins in the SOM were first described by King and Barker (1988) using gravity anomalies that depict values below 40 mGal. However, the gravity data shown in that work did not cover the westernmost part of the SOM. Busetti et al. (2000) refined the position of these basins by analyzing seismic reflection data. The orientations of the basins coincide with two main structural domains: (a) An E-W orientated graben south of the islands, the so-called Newton Basin, filled with more than 4 km of sediments (Harrington et al., 1972) and associated with the Mesozoic forearc setting (King & Barker, 1988). (b) N-S orientated grabens, located in the southern part of the SOM, the Airy, Bouguer and Eötvös Basins. Their formation is associated with east-west extension related to the separation of the SOM from the Antarctic Peninsula (King & Barker, 1988). The sedimentary infill of the SOM basins has been targeted by the Ocean Drilling Program (ODP) Leg 113 (P. E. Barker et al., 1988) that recovered sediment cores at Sites 695 and 696 (Figure 2). Site 695 reached upper Miocene sediments, while Site 696 recovered sediments spanning from the Eocene to the Quaternary (P. E. Barker et al., 1988). Recovered sediment cores record the evolution of the SOM from when it was attached to the Antarctic Peninsula to its present position. Before late Eocene (~37.6–35.5 Ma), locally sourced terrigenous sediments recovered at Site 696 are associated with the SOM still close to the Antarctic Peninsula (López-Quirós et al., 2021). The decrease in the input of these proximal sediments to the Site 696 is interpreted to indicate the separation between the SOM and the Antarctic Peninsula as a result of the proto-Powell Basin opening (López-Quirós et al., 2021). A terrestrial cooling phase at the latest Eocene (35.5 Ma) is also linked to the opening of the Powell Basin (Thompson et al., 2022).

3. Data and Methodology

This section describes the initial geophysical data used and the methodology leading to the construction of the 3D model validated by forward and joint inversion of gravity and magnetic data.

3.1. Initial Data Set

Bathymetric data of the study area has been extracted from the GEBCO 2020 database (GEBCO Compilation Group, 2020), which includes the IBCSO database (Arndt et al., 2013), with a cell resolution of 500 m (Figure 3a). The bathymetry of the SOM ranges from <500 m below sea level (mbsl) in the northern and the western area, deepening to the SE where the platform reaches depths up to 1,500 mbsl. The South Orkney Islands emerge toward the NNW limit of the SOM. To the north, the edge of the microcontinent is marked by the Orkney Trench, which deepens to up to 5,500 mbsl, along the South Scotia Ridge (SSR). The other margins show smoother slopes, reaching 3,000 mbsl. The 2,000 mbsl isobath (Figure 3a) has been considered to be representative of the continental area of the SOM, and has therefore been used as a visual reference in the figures throughout the work.

Multichannel seismic reflection (MCS) profiles cover most of the SOM (Figure 3a). The Seismic Data Library System (SDLS) provides an open database including profiles carried out by the Italian National Institute of Oceanography (OGS, 1989 and 1991), the Russian Polar Marine Geosurvey Expedition (PMGE, 1994), the British Antarctic Survey (BAS, 1985) and the Antarctic Spanish program (SCAN, 2001 and 2004). SDLS profiles were complemented by recently obtained MCS data collected by the Antarctic Spanish Program during the POWELL2020 cruise. The penetration of the MCS ranges from 4 to 8 s in TWTT (two-way travel time), allowing to image the acoustic basement in most cases.

The global GEMMA earth crustal model (Reguzzoni & Sampietro, 2015) offers a first approximation to the Moho depth in the area (Figure 5c). This model is calculated from GOCE satellite gravity data that provides a

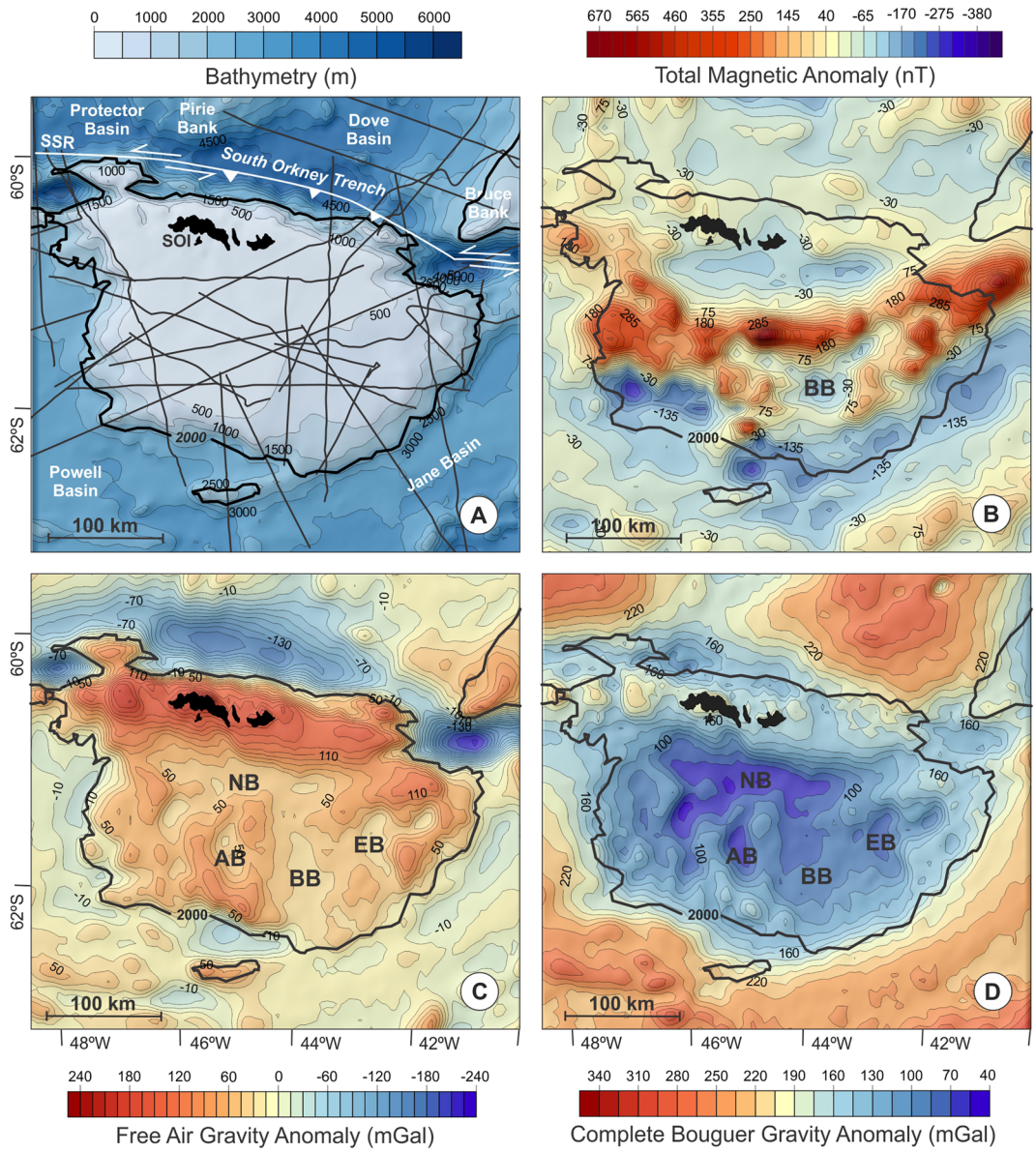

Figure 3. Initial data set used: (a) GEBCO bathymetry (GEBCO Compilation Group, 2020) with SDLS and POWELL2020 MCS profiles. (b) WDMAM total magnetic anomaly map with contour lines every 50 nT (Lesur et al., 2016). (c) Free-air gravity anomaly map with contour lines every 15 mGal (Sandwell et al., 2014). (d) Calculated complete Bouguer gravity anomaly map with contour lines every 15 mGal. The 2,000 m isobath is highlighted as a visual reference. The sedimentary basins are named by their acronyms: NB, Newton Basin; AB, Airy Basin; BB, Bouguer Basin; EB, Eötvös Basin.

global estimation of the mean Moho depth with a resolution of 0.5°. The GEMMA model shows a maximum Moho depth of 32.5 km under the central south area of the SOM and thins toward the edges of the SOM, reaching depths between 20 and 25 km. Below the oceanic crust of the Powell, Jane, Protector and Dove Basins, the Moho is modeled at depths between 11 and 15 km. GEMMA model describes a significantly deeper Moho than modeled in previously published work (Busetti et al., 2000; Kavoun & Vinnikovskaya, 1994; King & Barker, 1988).

The gravity anomaly data (Figure 3c) used for modeling were compiled from the global marine gravity database from Sandwell et al. (2014), and represents a free-air gravity data set with 1-min grid resolution. This global marine gravity model achieves twice the accuracy of previous models by enhancing existing data with new radar altimeter measurements from the CryoSat-2 and Jason-1 satellites (Sandwell et al., 2014; Smith & Sandwell, 1997). Gravity free-air anomaly values range from −230 to +240 mGal. A continuous east-west band

of negative anomalies at the north of the SOM, from −80 to −230 mGal, coincides with the Orkney Trench. The highest positive anomaly values ranging from 150 to 240 mGal, are found in the north of the SOM, where the South Orkney Islands are located. In the inner part of the SOM, free-air anomaly values ranging between 15 and 50 mGal, ∼40 mGal below the adjacent areas, can be highlighted (Figure 3c) related to the sedimentary basins (Busetti et al., 2000; King & Barker, 1988). In addition, we calculated the complete Bouguer gravity anomaly (Figure 3d) form the free-air gravity data set. For Bouguer plate correction we used a Bouguer density of 1.64 (2.67 gr/cm^3 as the mean crustal density and 1.03 g/cm^3 as water density). For terrain correction we used the bathymetry of Dickens et al. (2014) for local correction, which improves the resolution to 300 m on the continental shelf, and GEBCO for regional correction. The complete Bouguer gravity data allow to distinguish more clearly the position of the sedimentary basins and the boundary between the continental crust of the SOM and the adjacent oceanic crust.

Magnetic data were extracted from the World Digital Magnetic Anomaly Map (WDMAM) (Figure 3b), a global near-surface magnetic data compilation grid with a cell size resolution of 5 km (Lesur et al., 2016). The WDMAM database is composed of marine and terrestrial data. The data used in this work are mainly marine and therefore referenced to sea level. A band of positive magnetic anomalies is observed in the SSW-NNE direction over the SOM, reaching +700 nT in the center of the SOM. This band depicts continuously over most of the microcontinent, showing a discontinuity over the Bouguer sedimentary basin, where a relative minimum is observed.

3.2. Modeling

The building of a robust 3D geologic model of the SOM based only on the available data is not feasible due to their scarcity. Therefore, we choose three main geological boundaries as initial constraints to reduce the multiplicity of the modeling results: (a) the acoustic basement depth, (b) the PMA source boundary, and (c) the Moho. The estimation of these boundaries deduced from geophysical data, together with the bathymetry, have been used as constraints for 2D geological models, which in turn are the basis for the construction of the 3D model. The 3D geological model of the SOM has been improved and validated by forward modeling and joint inversion of potential fields.

3.2.1. Identification of the Main Geological Boundaries as Initial Constraints

As a first approach to the boundary between the sedimentary infill and the continental basement of the SOM, we mapped the acoustic basement from MCS profiles. The acoustic basement was manually identified and picked in the KINGDOM Suite software along each MCS profile (Figure 3a). The resulting depth grid (Figure 5a) is achieved through a double time-to-depth conversion, assigning velocities of 1,460 and 2,200 m/s (King et al., 1997) to the water and sediment layers, respectively.

The analytic signal (AS) has proven to be an effective tool for locating geological boundaries of the magnetic source bodies (Dentith & Mudge, 2014; Doo et al., 2009). The AS is defined as the square root of the sum of squares of the data derivatives in the x, y, and z directions (Roest & Pilkington, 1993; Roest et al., 1992). In this study, we calculate the AS from the WDMAM magnetic anomaly data using the GRIDASIG GX module of the Oasis Montaj software in order to locate the edges of the PMA source (Figure 5b).

The global GEMMA model (Reguzzoni & Sampietro, 2015) is a useful first reference model for crustal thickness variation (Figure 5c). However, the Moho depth below the SOM extracted from this model seems to be overestimated compared to the results previously described in the literature (Kavoun & Vinnikovskaya, 1994; King & Barker, 1988; Trouw et al., 1997). As a second approach, we have calculated the depth of the Moho below the SOM under isostatic equilibrium conditions (Figure 5d). We assess the theoretical isostatic root using the AIRYROOT GX module of Oasis Montaj based on the USGS algorithm by Simpson et al. (1983). This program calculates a Moho depth -the root-using the bathymetric grid, a crust-mantle density contrast and a compensation depth. We use the density contrast calculated from the difference between estimated densities of the mantle (3.3 g/cm^3) and the crust (2.67 g/cm^3): 0.63 g/cm^3. The compensation depth has been assumed at 27 km, as the thickness of the continental crust has been described in previous works to be no more than 26 km (see Section 2). For our study, we consider only the results in areas below the SOM since the values used for its calculation were based on continental crust (Figure 5d).

3.2.2. 2D Geophysical Modeling

The GM-SYS software (Gemperle et al., 1991), implemented in the Geosoft Oasis Montaj software, allows the building of 2¾-D models. The modeling takes into account the influence of adjacent bodies orthogonal to the

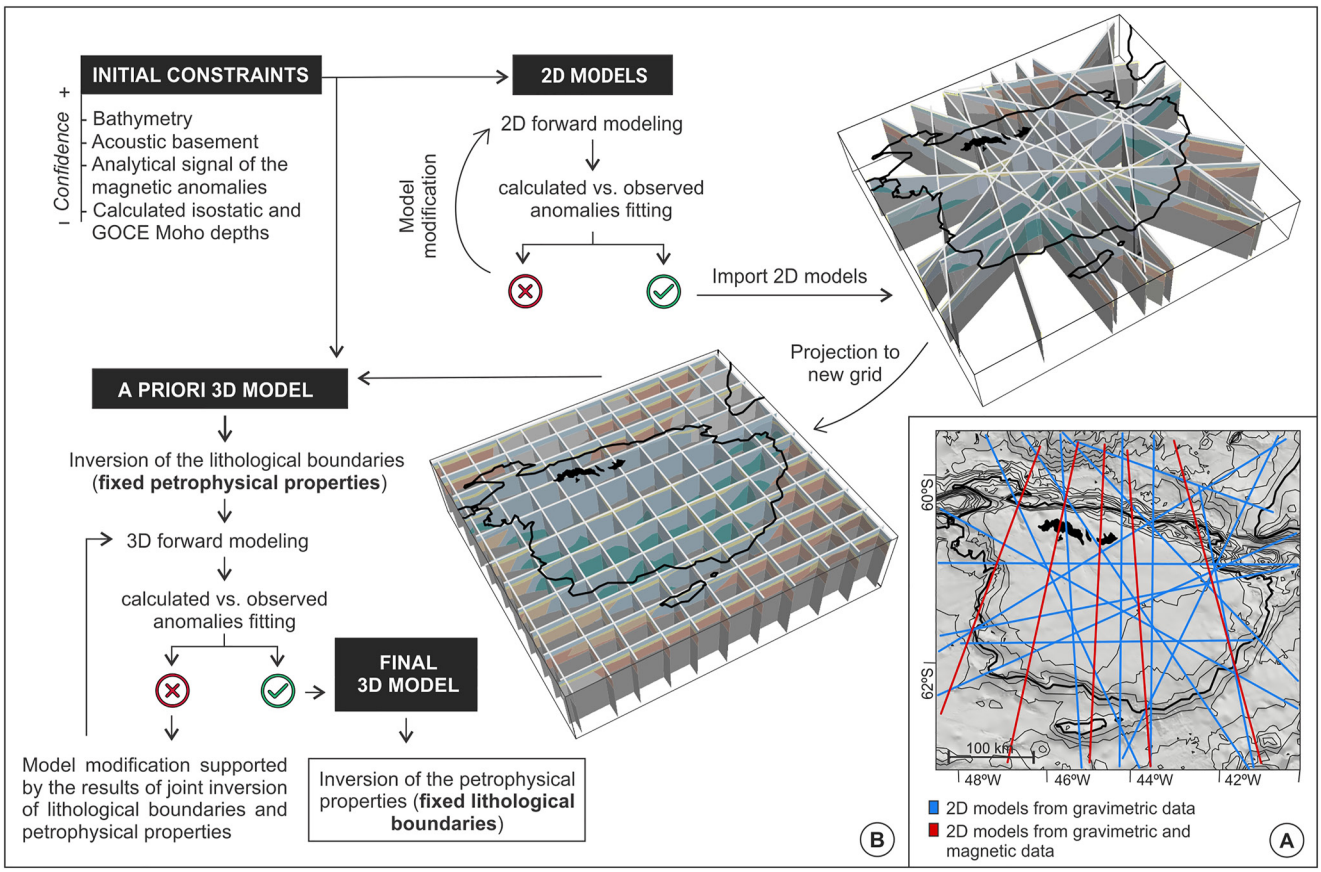

Figure 4. (a) Location of 2D models. In blue, the position of the gravity anomaly models, which correspond to the location of the dense network of MCS profiles extended to the limits of the modeling area. In red, the position of the profiles where simultaneous gravity and magnetic anomaly modeling has been performed. (b) Summary of the workflow followed for the modeling. Initial constraints were considered during 2D and 3D modeling.

profile for a defined extent (Northwest Geophysical Associates, 2004). For ease of reading, we refer to the models simply as 2D. We carried out 2D models of potential field data in order to locate the geological units of the SOM in depth. The main challenge in potential field modeling is that multiple sources with varying geometry and properties can fit the observed anomalies equally well. Due to the high reliability of the MCS data, 2D gravity models were fitted along 15 selected nearly rectilinear seismic profiles (blue lines in Figure 4a). To avoid edge effects, the profiles were extended to the limits of the selected study area. During 2D modeling, bathymetry was imported as a fixed surface. The calculated depth of the acoustic basement was considered a reliable surface in the areas with good quality of the MCS profiles (i.e., the Bouguer and Eötvös Basins mainly) (dotted line in Figure 5e). In the remaining modeled area, the acoustic basement was considered as a tentative input data. The Moho depth -isostatic and GEMMA- and the extent of the magnetic bodies were considered as guiding initial data. Once the gravity anomaly has been fitted along all selected seismic profiles, the gravity and magnetic anomalies are simultaneously fitted along five profiles (red lines in Figure 4a) perpendicular to the dipole (Figure 3b). In the case of magnetic anomalies, we only assign a magnetic susceptibility value to the batholith in order to adjust the low frequency anomalies. This allows to improve the geometry of the intrusive igneous rock body that cause the PMA. The aim of the modeling along the 2D profiles was to provide simple input surfaces for the 3D model, which resulted in a poorer fit of the anomalies.

3.2.3. 3D Geological Model: Geophysical Forward Modeling and Joint-Inversion

To define the geological structure of the SOM, we transfer the geological contacts from the 2D models to the corresponding vertical sections in Geomodeler software (Intrepid Geophysics) (Figure 4b). The 3D model extent is 440 km in the E-W direction, 410 km in the N-S direction and 40 km deep. Geomodeler builds the model using the principles of potential-field interpolation method (Calcagno et al., 2008; Lajaunie et al., 1997). Due to the

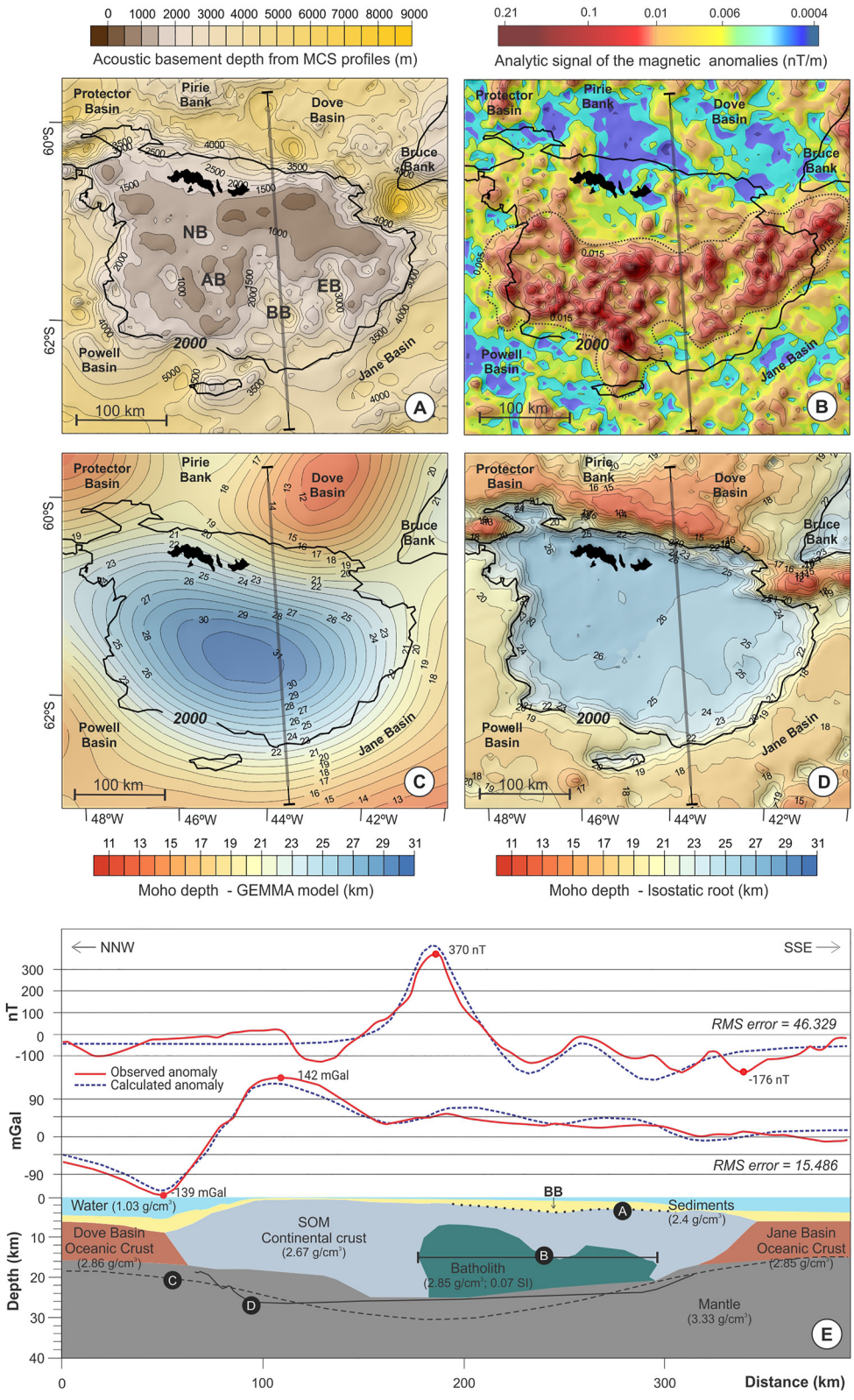

Figure 5.

irregular distribution of the 2D models (see Figure 4a), the first 3D model portrayed many inconsistencies. To solve this, we created an additional grid composed of evenly spaced N-S and E-W vertical sections (Figure 4b), where the structures were projected to ease the modification of the interfaces of the lithological units. The interpolation of all imported data constitutes our initial 3D geological model, the "a priori" 3D model (Figure 4b).

Geophysical forward modeling and inversion were implemented to refine the "a priori" 3D model. Forward modeling computes the gravity and magnetic response taking into account uniform petrophysical properties values. Joint inversion discretizes the geological model into a 3D matrix of voxels. In this study, voxels have an extension of 10 km in *xy* directions. In the *z*-direction, the software allows to define a voxel geometry in which the cell size can vary with depth. The cell size in *z*-direction has a fixed value above a certain boundary. Below this boundary, the cell size increase by a defined factor. In this case, we set a cell size of 200 m from the sea level to 20 km depth. Below 20 km depth, this value starts to increase by a factor of 1.3 ending in a last cell with a size in *z*-direction of 4.65 km. For each voxel, the software can modify the petrophysical properties (i.e., density and magnetic susceptibility) and/or lithological boundaries according to defined probability functions. In addition, the user can set the degree of freedom allowed to the software (very tight, moderate or loose) for each boundary between lithological units (Calcagno et al., 2008). Inversions that we carried out ran for 2 million iterations. Throughout the modeling process, the bathymetry was established as a fixed surface. The acoustic basement was also considered fixed in those areas where it could be defined with confidence (i.e., Bouguer and Eötvös Basins).

In a first stage, the goal was to obtain a geologically robust model that conforms to the regional geodynamic framework, especially in the areas not covered by the 2D models. For this purpose, we performed a joint inversion with fixed petrophysical properties and moderate degree of freedom allowed for lithological boundaries to improve the geometry of the model "a priori" (Figure 4b). The geologically consistent proposed changes that improved the adjustment were accepted. To refine the geometry of the model in detail, forward modeling was best suited. In areas where differences between computed and observed data were localized, the lithological boundaries were modified by trial-and-error to improve the fit. This process was complemented with several joint inversions of the lithological boundaries and petrophysical properties simultaneously and with equal weighting of probability functions for both. The inversion returns changes in lithological boundaries and the most likely distribution of petrophysical properties. The final geometry was reached when the applied changes no longer significantly improved the forward modeling result. At this point, the final model represents the geological structures realistically and does not present inconsistencies. The last stage consists of an inversion of the petrophysical properties with fixed geometry of the different lithological units (Figure 4b). After the last stage of the inversion process (Figure 4b), a more realistic configuration of the density variability and magnetic susceptibility is achieved (Figures 6f and 7f). The RMS error of the misfits between the observed and calculated anomaly is substantially improved compared to forward modeling (see Section 4.2).

4. Results

The results obtained during the modeling include: the geological boundaries used as constraints (see Section 3.2.1), the fit achieved in the 2D and 3D models and the geometry of the final 3D geological model. In this section we have highlighted the three main surfaces that will be discussed below.

4.1. Initial Surfaces and 2D Models

The acoustic basement depth, calculated from seismic data, ranges from 382 mbsl at the northern SOM to 9,000 mbsl in the Orkney trench and provides a first approximation to the location and geometry of the sedimentary basins (Figure 5a). The reliability of the grid is limited to areas with good MCS data coverage (Figure 3a). For example, the greatest acoustic basement depths within the continental shelf coincide with well surveyed position of the Bouguer (4,200 mbsl) and Eötvös (3,500 mbsl) Basins. Instead, the less surveyed area of the Airy Basin

Figure 5. (a) Acoustic basement depth derived from MCS profiles with contour lines every 500 m. The sedimentary basins are named by their acronyms: NB, Newton Basin; AB, Airy Basin; BB, Bouguer Basin; EB, Eötvös Basin. (b) Analytic signal of the total magnetic anomaly with contour lines every 0.005 nT/m. The most probable zone for the presence of the batholith is outlined in dotted line. (c) Depth of the Moho from the GEMMA global model (Reguzzoni & Sampietro, 2015). Contour line every km. (d) Calculated Moho depth assuming an isostatic equilibrium. Contour line every kilometer. (e) Gravity and magnetic adjustment of a N-S oriented 2D model. The location of the profile is shown in panels (a–d). The acoustic basement, the extent of the PMA source and the GEMMA and Isostatic Moho are projected over the profile and labeled A–D. BB, Bouguer Basin.

10.1029/2022TC007602

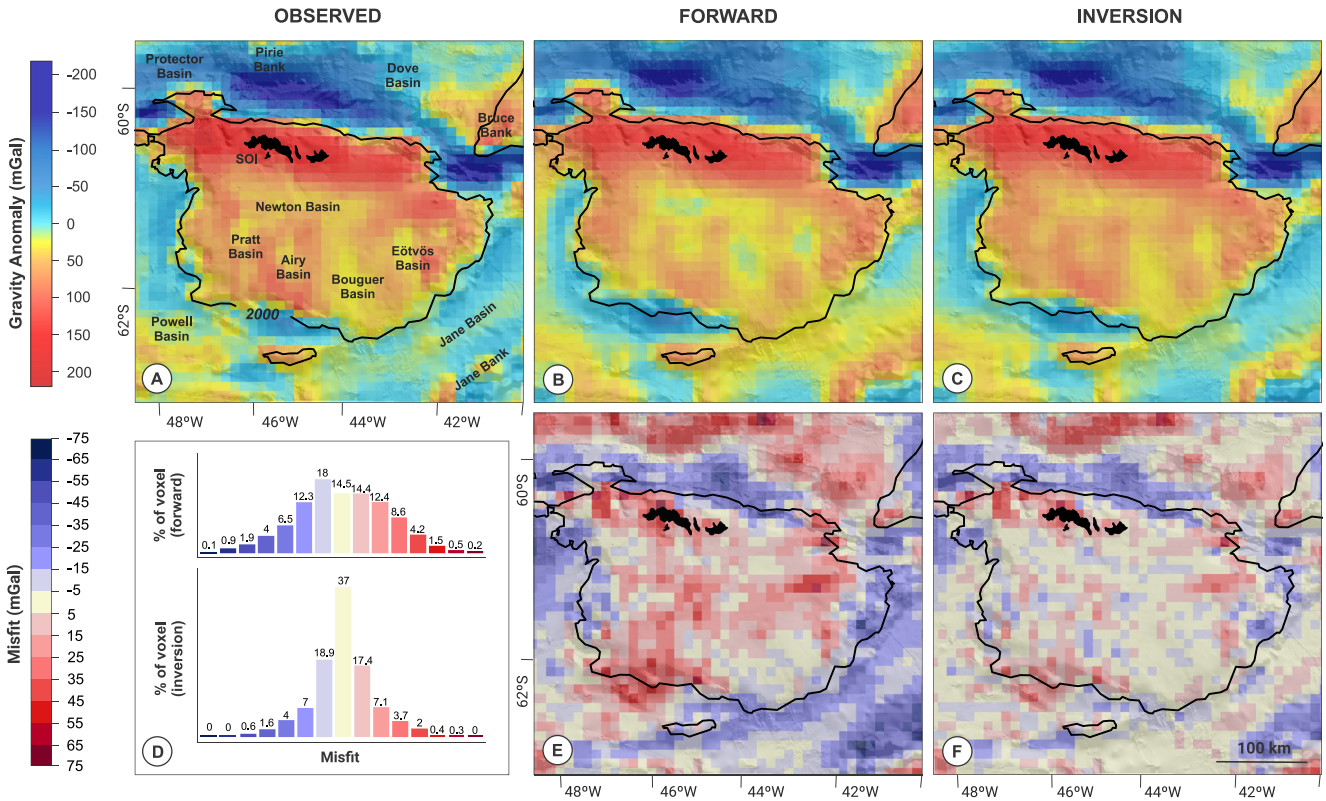

Figure 6. (a) Observed free-air gravity anomalies. Anomaly ranges may vary slightly from the original satellite data due to the gridding simplification. (b) Forward calculated gravity response of the final 3D model. (c) Gravity response of the final 3D model with inverted density values. (d) Histogram of misfit distribution in panel (e, above) and panel (f, below). (e) Misfit between forward gravity response and observed anomalies. (f) Misfit between inverted and observed gravity anomalies.

images a small depocenter surrounded by basement highs. To the west, another small depocenter is observed. The Newton basin is not recognized due to the poor quality of seismic profiles in this area.

The Analytic Signal (AS) amplitude calculated from magnetic anomalies ranges from 0 to 0.2 nT/m (Figure 5b). Higher AS amplitude corresponds to bodies closer to the surface whereas lower amplitude might correspond to bodies placed either at greater depth or to the absence of magnetic bodies (Hsu et al., 1998). The highest AS amplitude is located in the center of the SOM. We consider AS amplitudes >0.01 nT/m to frame the source of the magnetic anomalies. This area has been delimited as the most likely location of the PMA source (Figure 5b). According to the results, the intrusive igneous rock body causing the PMA (also called batholith this work) would be sited in the southern half of the microcontinent, extending to Bruce Bank.

The depth of the Moho calculated under isostatic equilibrium (Figure 5d) shows a crustal thickness that reaches 27 km below the islands. The crust thins toward the SE, where the bathymetry deepens, resulting in a Moho depth of 24 km below the Eötvös and Bouguer Basins. This result contrasts with the global GEMMA earth crustal model (Reguzzoni & Sampietro, 2015) (Figure 5c), where the maximum depth of the Moho of 31.5 km was located in the central area of the SOM and decreases toward the edges.

These three initial constraints provide the basis for the 2D modeling. Figure 5e shows one of the five 2D models realized fitted to the gravity and magnetic anomalies. The RMS error between the observed and calculated magnetic anomaly is 46 nT, within a range of the observed magnetic anomaly between −176 and 370 nT. For the gravity anomalies, the RMS error along this profile is of 15 mGal, and the minimum and maximum observed gravity anomalies are −140 mGal and 139 mGal, respectively. RMS errors present similar values for all the 2D models carried out.

Table 1
Petrophysical Properties of the Lithological Units Used for the 3D Forward and Inversion Modeling

	Forward		Inversion	
Lithological unit	Density (g/cm^3)	Magnetic susceptibility (SI)	Density variation (g/cm^3)	Magnetic susceptibility variation (SI)
Water	1.03	–	1.03	–
Sediments	2.4	–	2.4 ± 0.1	–
Oceanic Crust (*Dove, Protector, Jane, Powell Basins*)	2.85	0.03	2.85 ± 0.075	0.03 ± 0.007
Continental Crust (*Pirie Bank, Bruce Bank, SOM*)	2.7	0.007	2.7 ± 0.04	0.007 ± 0.004
Oceanic Crust (*Weddell Sea*)	2.9	0.03	2.9 ± 0.075	0.03 ± 0.007
Jane Bank	2.83	0.05	2.8 ± 0.07	0.05 ± 0.015
Thinned And Intruded Continental Crust (*Powell Basin*)	2.8	0.03	2.8 ± 0.02	0.03 ± 0.02
Intrusive body	2.88	0.07	2.88 ± 0.07	0.07 ± 0.05
Mantle	3.33	0	3.33 ± 0.035	0

4.2. Gravity and Magnetic Response of the Final 3D Geological Model

The final 3D geological model produces a gravity and magnetic response in forward modeling (Figures 6b and 7b) taking into account homogeneous petrophysical properties for each lithological unit (Table 1). During the inversion process, these fixed values are allowed to vary in a controlled range (Table 1). The fixed values used for the forward modeling and the ranges of variation used in the inversion modeling are chosen after the empirical values in Telford et al. (1990) and values previously used in models near the study area (Bohoyo, 2004; Busetti et al., 2000; Galindo-Zaldívar et al., 2006; Maldonado et al., 2014). The inversion of these petrophysical properties produced an improved gravity and magnetic response (Figures 6c and 7c).

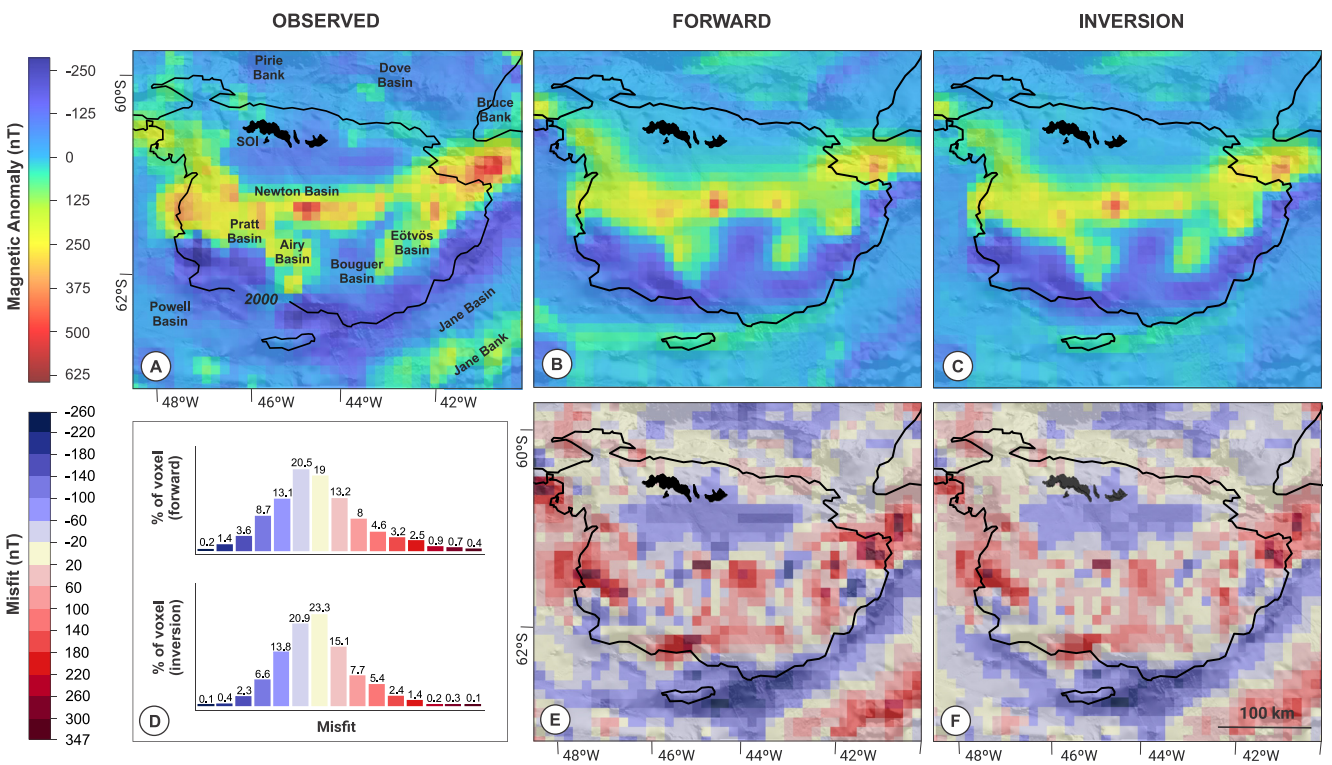

Figure 7. (a) Observed WDMAM magnetic anomalies. (b) Forward calculated magnetic anomalies of the final 3D model. (c) Calculated magnetic anomalies of the final 3D model with inverted magnetic susceptibilities. (d) Histogram of the misfit distribution in panel (e, above) and panel (f, below). (e) Misfit between forward magnetic and observed anomalies. (f) Misfit between inverted and observed magnetic anomalies.

The free-air gravity computed anomaly in the final forward modeling ranges from −185 to 161 mGal while the observed anomaly data ranges between −219 and 220 mGal. The misfits range between ±75 mGal. The forward model is able to describe the main features of the free-air anomalies, but the RMS error is still relatively large with 23.3 mGal. Larger differences can be observed at the northern boundary of the model: the Jane Bank, the contact between the SOM and Bruce Bank, and around the South Orkney Islands (Figure 6e). During modeling, the misfit values around the South Orkney Islands were expected to be high because the altimeter-derived gravity close to them is unreliable and over them it is absent. Within the SOM, the misfits were up to +50 mGal, being the southwest and the northeast border of the SOM the most conflictive areas. After the last stage of the inversion process, the variability applied to the density values resulted in a considerable improvement of the free-air gravity anomalies. At this point, the computed anomaly ranges between −189 and 164 mGal and the misfit values range between −53 and 60 mGal. The RMS error reduced to 15.8 mGal. It is noteworthy that the largest misfits in the forward were scattered over all the modeled area. After inversion, the greatest misfits are at the edges of the model, outside the SOM (Figure 6f). Figure 6d shows two histograms representing the distribution of misfits for forward and inversion modeling. The bars correspond to 10 mGal intervals with the same range and colors as the misfit color scale. The percentage of voxels with a misfit between 5 and −5 mGal improve from 14.5% to 37% after inversion (Figure 6d). This, together with the improvement of RMS errors provide good reliability in the model when discussing the results.

For the magnetic anomalies, we could not achieve a desirable adjustment. The forward response of the final 3D model ranges from −220 to 514 nT (Figure 7b) while the observed anomaly data ranges from −286 to 647 nT (Figure 7a), with an RMS error of 91.8 nT. After the last stage of the inversion process, the RMS reduces to 77 nT, which is still far from acceptable. In this case, moreover, the distribution of the misfits did not significantly improve after the inversion (Figure 7d). With a voxel dimension of 10 km in the *xy* direction, the high frequencies of magnetic anomalies were difficult to fit. Although the RMS error values were very high, the morphology of the computed anomalies and the position of the maximum values show a good match with the observed anomalies (Figures 7a–7c).

4.3. Sedimentary Basins of the South Orkney Microcontinent

The final geometry of the 3D model enables the analysis of the complete sedimentary cover of the SOM. These results are more reliable within the continental area of the SOM, associated in this work to the 2,000 m isobath (Figure 8a). To the north, the Newton Basin extends in an E-W direction for about 150 km and is 20 km wide. The depocenter is located at its western end and it is filled with a 3.5 km thick sediment cover. The morphology of the northern and southern boundaries of the Newton basin results in a boudinage shaped basin (Figure 8a). In the southern area, the Airy, Bouguer and Eötvös Basins have a N-S orientation (Figure 8a). According to the modeling results, the Airy Basin is framed by basement highs and has an ellipsoidal shape of 17 × 30 km, with a central depocenter accumulating 2.1 km of sediments. To the west of the Airy Basin, another elongated N-S basin is distinguished. Since it is sufficiently large, we tentatively name it Pratt Basin in this work (Figure 8a). Pratt Basin is about 70 km long and 25 km wide with a maximum sediment thickness of 2.4 km in the northern area. Eötvös and Bouguer Basins are located in the southeastern part of the SOM where the bathymetry is deeper. Both basins are separated by a relative basement high and widen southeast. Sedimentary thickness in the Bouguer Basin reaches 2.9 km. Eötvös Basin has a thickness of 2.8 km in its deepest area. To the east of this basin, there is another depocenter, which is 2.1 km thick. The ODP Site 696 was drilled in the southern edge of the Eötvös Basin (Figure 2) where, according to the model, the basin accumulates 1.6 km of sediments.

4.4. Characterization of the Intrusive Igneous Rock Body Causing the PMA

The modeled body of intrusive igneous rock causing the PMA, also called batholith in this work, is located in the southern area of the SOM and present variable thickness (Figure 8b). The maximum thicknesses are found in the central SOM, matching the area of basement highs surrounding the Airy Basin. In this area, the body portrays thickness between 15 and 20 km, where the magnetic maximum is also located. It is an elongated magnetic province about 130 km wide that extends throughout the southern part of the SOM and continues eastwards out of the modeling area. The body ends at the edge of the Powell Basin. The interruption of the batholith coinciding with the position of the Bouguer and Eötvös Basins is noteworthy.

10.1029/2022TC007602

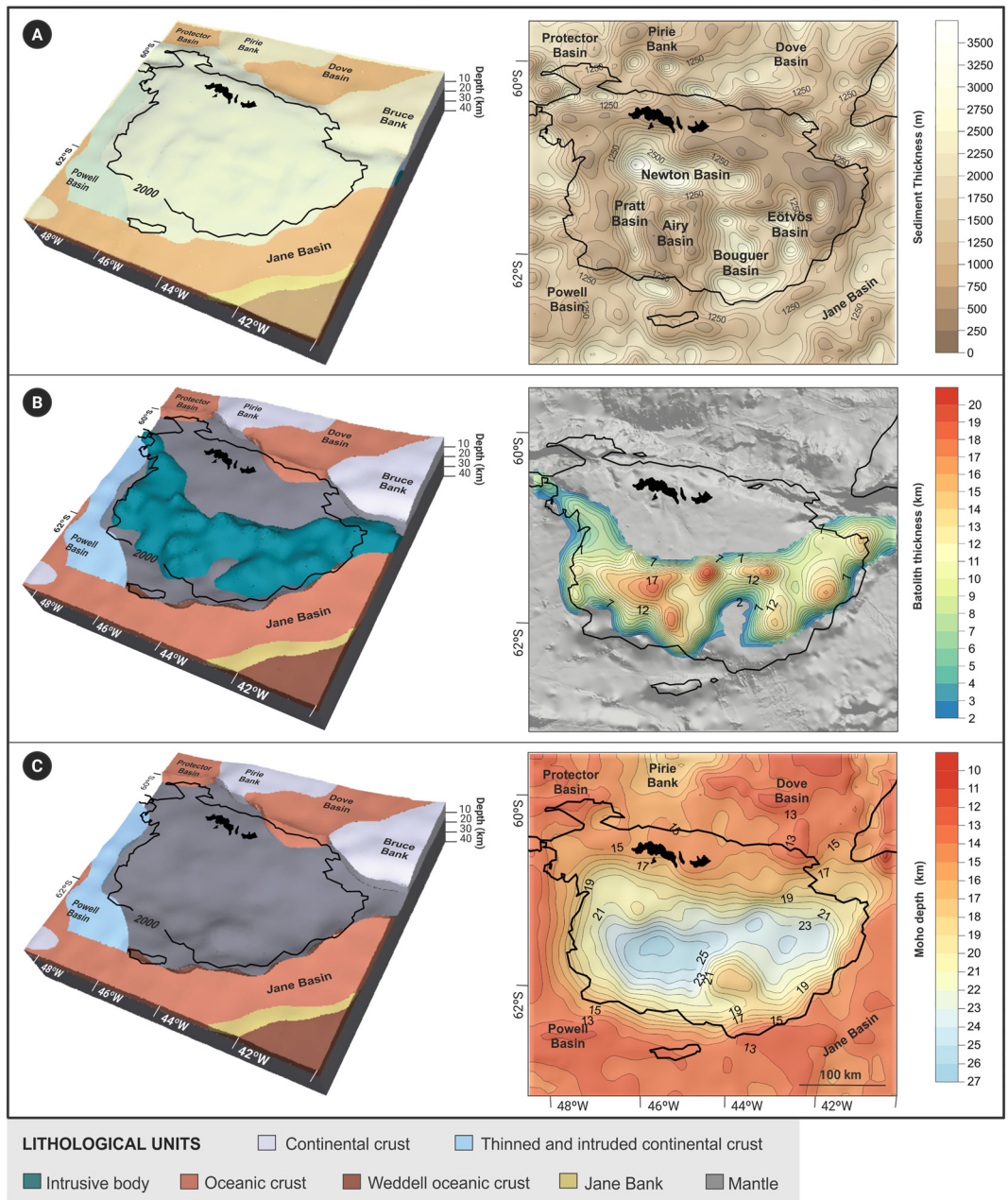

Figure 8. Main results derived from the 3D modeling. For better visualization, 3D volumes and contour maps are shown for each unit of interest: (a) Sedimentary cover thickness. The volume of the 3D sedimentary cover is shown with transparency. Contour lines every 250 m. The 1,500 m isopach is highlighted. (b) Batholitic complex. Contour lines every kilometer. (c) Moho depth. Contour lines every kilometer. The vertical exaggeration of the 3D model is 2.

4.5. Moho Depth

Although we considered two different models of Moho depth (the global GEMMA model and the calculated isostatic Moho depth) as a starting point, the result of the 3D modeling (Figure 8c) shows that both were overestimated. The result of the Moho depth derived from the 3D model below the oceanic crust of Protector, Dove, Powell and Jane Basins ranges from 10 to 13 km. This depth increases to 18 km under the Pirie and Bruce Bank continental blocks. Under the continental area of the SOM, three zones can be distinguished: (a) the northern sector, where the Moho depth ranges between 15 and 20 km; (b) the south-western sector, where the greatest

crustal thickness places the Moho at 26.5 km; and (c) the south-eastern sector, characterized by the shallowing of the Moho to 17.5 km depth, coinciding with the modeled interruption of the batholith.

McKenzie (1978) first introduced the stretching factor β to describe the formation of intracontinental rift basins by rapid stretching of the lithosphere. The stretching factor β has also been used to define the extension occurring in the whole crust (Chen, 2014; Zhang et al., 2008). The stretching factor β can be calculated through formula $\beta = ct_0/ct_{now}$, of which, ct_0 is the original thickness of the crust, and ct_{now} is the thickness of present crust (Alvey et al., 2008). A thinned crust presents higher values of stretching factor β. To produce a sedimentary basin filled with 4.5 km of sediments requires a stretching factor β of about 2 (McKenzie, 1978). We have calculated an estimation of the stretching factor β from the model results. To do this, we need to assume the original thickness of the crust. Garrett (1990) performed two-dimensional models of the crustal structure of the Antarctic Peninsula that described a crustal thickness of about 30 km. If we take this value as the assumed original thickness of the SOM crust, β would have a value of 1.13 for the south-western sector of the SOM, and a value of 1.71 for the south-eastern sector.

5. Discussion

The results derived from the 3D model provides improved insight into the geological structure and evolution of the South Orkney Microcontinent which have tectonic implications for the early stages of the Scotia Arc development.

5.1. 3D Geophysical and Geological Modeling as a Suitable Method to Characterize and to Understand Deep Structures

The 3D geological model of the SOM was built by combining acquired geophysical data and calculated data of its deep structure with gravity and magnetic data. The approximation in depth of the different geological contacts prior to modeling has allowed the results to be geologically consistent. After the joint inversion of the petrophysical properties of the final 3D geological model, there were differences between the fit achieved in the gravity and the magnetic anomalies. In the case of the gravity anomalies, the RMS error achieved is 15.8 mGal. Given the complexity of the area and the relative simplicity of the model in terms of lithological units involved, we consider that the final geometry and the distribution of density values represent the SOM structure in a realistic way. In contrast, the fit to the magnetic anomalies is not satisfactory, presenting a RMS error of 77 nT. However, the approximation to the shape of the magnetic anomalies was quite accurate (Figure 7c). In fact, we believe that it was decisive to take into account the AS of the magnetic anomalies as a guide during the modeling process. This permitted to delineate the PMA source. If the magnetic component had not been taken into account, the gravity anomalies could have been misinterpreted, as the batholith is dense and very bulky. The final range of densities attributed to the batholith is within the range of densities of gabbros (2.70–3.11 g/cm^3 in Telford et al. (1990)), which is the composition previously described in the literature (Garrett et al., 1986/87).

The modeling carried out in this study proved to be very effective for the characterization of the sedimentary cover. Most of the SOM sedimentary basins were previously located by King and Barker (1988) and roughly described by Busetti et al. (2000). In the present study, by combining the analysis of the available seismic profiles with the gravity modeling, the position and geometry of the basins has been determined more precisely and the total sediment fill thickness has been estimated for the first time. The Eötvös, Bouguer and Airy Basins are easily identifiable from seismic data and their depths can be mostly estimated directly. To the west of the Airy Basin, another elongated N-S basin, here named Pratt Basin, is noteworthy. This basin was not identified in the previous description of the SOM sedimentary infill of King and Barker (1988) due to lack of gravity data coverage in this area. However, they analyzed a seismic profile in the surroundings of this basin (profile "E" in King and Barker (1988)) and described the presence of normal faults and sedimentary fill. Busetti et al. (2000) mapped the basin depocenter (Figure 2) but its shape could not be delimited. Similarly, a small basin to the east of the Eötvös Basin was included as part of the Eötvös Basin in the work of King and Barker (1988), but our results show that it is another disconnected basin (Figure 8a). On the other hand, the sparse coverage of the Newton Basin with seismic profiles leads to an underestimation of the sediment thickness. In fact, gravity anomalies reveal that Newton Basin might be deeper than initially observed. Based on the model, sediment thickness in the Newton Basin is up to 3.5 km, which is closer to the more than 4 km described by Harrington et al. (1972) by means of the seismic refraction profile performed west of the South Orkney islands.

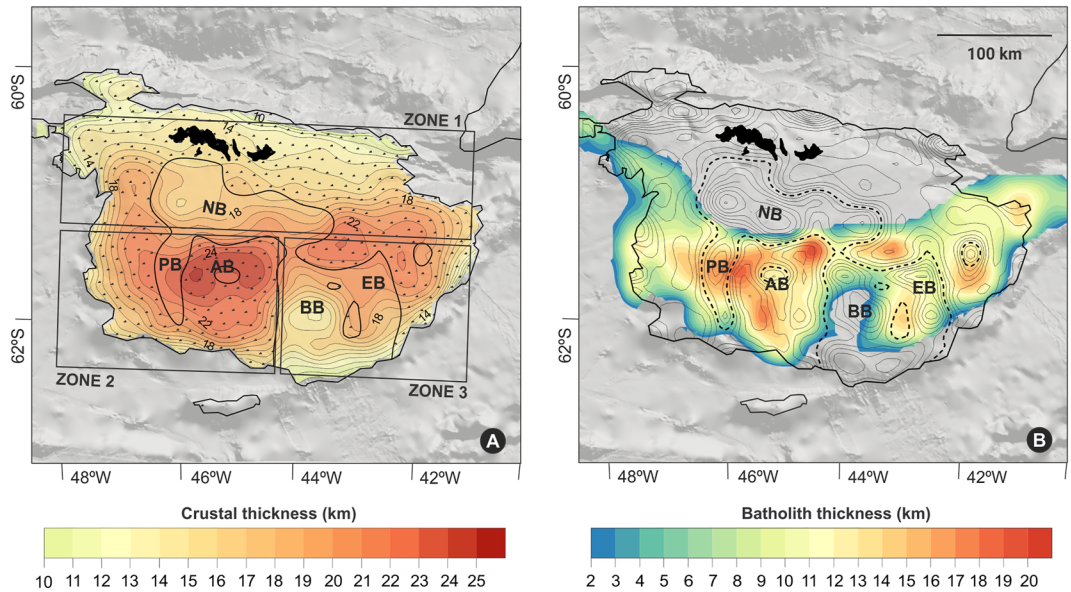

Figure 9. (a) Differentiated zones in the SOM according to the thickness of the crust. The dotted area frames the structural highs according to the model results. (b) Superposition of batholith thickness variation and location of the sedimentary basins. The 1,500 m isopach of the sedimentary cover is highlighted to delimitate the sedimentary basins. Sedimentary basins are identified by their acronyms: AB, Airy Basin; BB, Bouguer Basin; EB, Eötvös Basin; PB, Pratt Basin.

5.2. Structural Heterogeneity of the South Orkney Microcontinent

The crustal thickness heterogeneity of the SOM is consistent with a complex tectonic evolution. According to the results derived from the model, we can distinguish three zones (Figure 9a). The northern third of the SOM, zone 1 in Figure 9a, clearly shows a crustal thinning. The difference in Moho depth between the model results (Figure 8c) and the theoretical calculation under isostatic equilibrium conditions (Figure 5d) in this area is up to 10 km. However, this difference is much smaller in the southern SOM. This is consistent with the conclusion reached by King and Barker (1988) that the continental block of the SOM is mostly in isostatic equilibrium except for the northern part. The most likely reason, given the position of the northern margin, is an uplift of the northern sector of the SOM, related to the active strike-slip movement with compressive character along this South Scotia Ridge segment (Bohoyo et al., 2007).

Early Cretaceous intrusive igneous rock bodies produced major crustal growth on the western Antarctic Peninsula and they are an important component of the continental crust in the area (Vaughan et al., 1998). Likewise, in the southern half of the SOM, the crust is thickened by the presence of the batholith (Figure 9). King and Barker (1988) in the description of the tectonic fabric of the southern portion of the SOM, identified two extensional systems separated by a central horst representing the only portion not affected by stretching. Based on our results, however, we distinguished two zones in the southern area of the SOM (Figure 9a). The zone 2 (Figure 9a), to the west, concentrates the greatest crustal thickness, which may therefore have been less affected by extensional processes. In zone 3 (Figure 9a), to the east, the absence of the batholith coincides with an extreme crustal thinning that must be the result of further extension of this zone (Figure 9a). This extension is also recorded by the bathymetry since the southeastern part of the SOM is where the deepest water depth is located (Dickens et al., 2014). Thus, we conclude that the whole south sector is affected by extensional tectonism, with increasing intensity toward the east.

The differentiation between zone 2 and zone 3 (Figure 9a) is also reflected in the position of the sedimentary basins and its relation with the thickness variation of the batholith. The discontinuity observed in the batholith match the location of the most important sedimentary basins, the Bouguer and Eötvös Basins (Figure 9b). The opening of the narrower Airy and Pratt Basins also coincides with regions of an evident thinning of the batholith (Figure 9b). In addition, the horsts surrounding the Airy basin are located where the batholith is thickest (Figure 9b). Therefore, we interpret that the batholith has thinned as a result of the opening of the N-S elongated basins that even produced its fracturing under the Bouguer and Eötvös Basins. Moreover, the E-W extension

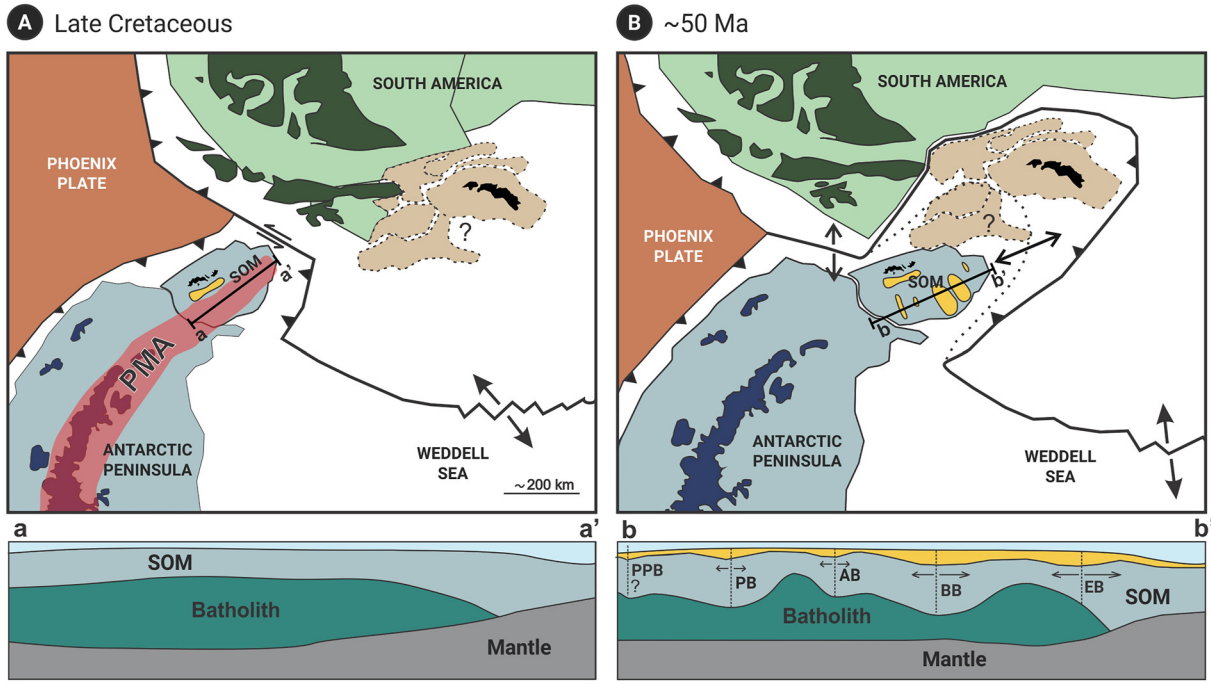

Figure 10. Sketch of the different phases of the SOM tectonic evolution. (a) Late Cretaceous: Subduction of the Phoenix Plate below the Antarctic Peninsula producing the intrusion of the batholitic complex. (b) Around 50 Ma: Beginning of the extension to the east of the SOM that causes the opening of the N-S elongated basin. AB, Airy Basin; BB, Bouguer Basin; EB, Eötvös Basin; PB, Pratt Basin; PPB, Proto-Powell Basin. Kinematic reconstruction after van de Lagemaat et al. (2021).

affecting the SOM and leading to the opening of the N-S elongated sedimentary basins (Pratt, Airy, Bouguer and Eötvös) seems to have been greater in zone 3. The estimated values for the stretching factor can be related to the thicknesses of the sedimentary basins in these areas (see Section 4.5). Zone 3, with the greatest stretching factor β of 1.71 corresponds to the Bouguer and Eötvös Basins that accumulate up to 2,800 m of sediments. Zone two, with an estimated stretching factor β value of 1.13, has a sedimentary thickness of up to 2,400 m in the Pratt basin. This configuration could be associated with an extensional process that began east of the SOM and migrated westward later.

The E-W extensional regime must have affected the entire SOM in a similar way. However, it is noteworthy that no features associated with this extension are well observed in the northern area. One possibility is that the Newton Basin was originally smaller than present and the E-W extension enlarged its geometry, creating the boudinage pattern that is shown by the 1,500 m sediment isopach (Figure 8a). Otherwise, the two domains (north and south) should be separated by a tectonic feature, such as a strike-slip fault, which decouples the deformation. In the southern SOM, however, deformation appears to be coupled throughout the crustal thickness, taking into account the above-mentioned correlation between shallow and deep features. This could be conditioned by the rheology of the different layers of the lithosphere. The depth at which the lithosphere changes from brittle to ductile behavior, the "brittle-ductile transition" of Kirby (1983) is greater in basic rocks than in acidic rocks (Ranalli & Murphy, 1987). Therefore, the basic nature of the batholith could have facilitated its fracturing together with the opening of the N-S elongated basins.

5.3. Regional Tectonic Implications

The results derived from the model have implications for the tectonic processes involved in the formation of the sedimentary basins of the SOM. Previous works interpreted the Newton Basin as an intra- or fore-arc Cretaceous basin based on the compatibility between the direction of extension and the orientation of the intrusive basic igneous body causing the PMA (Eagles & Livermore, 2002; King & Barker, 1988). Our model results are compatible with the interpretation of the Newton Basin as a fore-arc basin originated during the Late Cretaceous, contemporary with the emplacement of the batholith (Figure 10a). The boudinage pattern in the 1,500 m isopach

of the Newton basin (Figure 8a) could be related to the prolongation of the extension of the N-S elongated basins northward or be the result of E-W extension of basement.

The results obtained from the 3D modeling and some geological assumptions allow us to propose a relative age for the opening of the Bouguer, Eötvös, and Airy Basin, which would also apply to the Pratt Basin identified in this work. The correlation between the thinning and fragmentation of the batholith with the position of the N-S elongated basins (Pratt, Airy, Bouguer and Eötvös) (Figure 9b) leads us to assume a basins formation age younger than the intrusion. To further constrain the age of formation of these basins, we turn to the sedimentary record recovered from the ODP Site 696, drilled on the Eötvös Basin (P. E. Barker et al., 1988). The deepest sedimentary section of ODP Site 696 is attributed to the late Eocene (~37.6–35.5 Ma). Below the lowest sediments recovered at ODP site 696, our model and seismic data show that there are further 955 m sediments to reach the basement. The similarity between the late Eocene depositional environment and sediment composition of SOM and Seymour Island suggested to López-Quirós et al. (2021) that the SOM was sourced by sediment from the Antarctic Peninsula, to which it was still attached or in close proximity at that age. Interpolating the sedimentation rate of ~4 cm/kyr calculated for the lower sediments recovered from ODP Site 696 (López-Quirós et al., 2021) to the additional unsampled sediment thickness below the site, we could assign an age of about 58 Ma for the sediments resting directly above the basement. However, this age is speculative as sedimentation rates can be expected to have changed over time. More reliable sedimentation rates are calculated from the Seymour Island formations, which span from the Cretaceous to Eocene. In Seymour Island, sedimentation rates in sedimentary units older than 37.6 Ma range between 5.5 and 7.6 cm/kyr (Amenábar et al., 2020; Bijl et al., 2013; Montes et al., 2019). If we consider similar sedimentation rates for SOM sediments older than late Eocene at Site 696, we could attribute ages between 45 and 50 Ma to the deepest sediments of the Eötvös Basin.

In this time frame, the initial development of the N-S elongated basins may be related to an early stage of the Scotia Arc formation before or around 50 Ma (Figure 10b). We interpret the differential deformation observed between the eastern and western sectors of the southern part of the SOM (Figure 9a) to be result of a great extensional stress to the east of the SOM, rather than two extensional systems separated by a central horst (King & Barker, 1988). The extension must have started east of the SOM, maybe linked to Weddell subduction below the east side of the Arc (Figure 10) and migrated westwards thereafter. A clear disconnection between the SOM and the Antarctic Peninsula has been interpreted at 35.5 Ma, during a Proto-Powell formation stage (López-Quirós et al., 2021; Thompson et al., 2022). However, the opening of the Powell Basin may have begun earlier. The alkali basalts dredged from the Antarctic Peninsula margin conjugated to the western SOM have Eocene age (47.7 and 49 Ma) (Barber et al., 1991). These dates fit within the proposed range for the start of sedimentation in the Eötvös Basin, suggesting that regional extension indeed affected the SOM and Powell Basin simultaneously. We postulate that a proto-Powell Basin existed parallel to the Pratt, Airy, Bouguer and Eötvös Basins (Figure 10b), which subsequently developed in a last stage finally becoming oceanic. The opening of the N-S elongated basins fits into a regional history of extensional deformation that begins with thick crust that as it extends thins in multiple places in a "core complex" mode. Subsequently, extension focuses on the Powell basin that deepens and widens to produce a crustal neck prior to seafloor extension.

6. Conclusions

The integration of observed and calculated geological and geophysical information with geophysical modeling of gravity and magnetic data has allowed the development of the first detailed geological 3D model of the SOM. The results of the modeling enable to link the deep structure of the SOM with its tectonic evolution. The following conclusions can be summarized from the research described above:

- 3D geophysical and geological modeling reveals as the most powerful tool for integrating different datasets to characterize large geological structures in regions with scarce direct data as Antarctica.
- In the absence of well distributed seismic information, 3D modeling of gravity anomalies enables to accurately define the geometry of sedimentary basins. In this work we have been able to determine the depth of the Newton Basin and define the existence of a well-developed sedimentary basin, the Pratt Basin.
- The N-S elongated basins (Pratt, Airy, Bouguer and Eötvös) were formed due to a great extensional stress during early stages of the Scotia Arc opening. Newton Basin could be slightly deformed and extended during the N-S elongated basin formation.

- The style of deformation undergone by the SOM is conditioned by the rheology of its different layers. The rheology of the batholith linked to its basic nature could have facilitated its brittle deformation coupled with the opening of the N-S elongated basins.
- The interrelated deformation observed in the structural features of the SOM suggest that the south-eastern area of the SOM has been the most affected by the eastwards tectonic extension. Extensional stress was greatest to the east of the SOM in the early stages of the Scotia Arc fragmentation, propagating westward thereafter.
- The Powell Basin may have been another N-S elongated basin to the west of the Pratt Basin, which may have progressed at a later stage, leading to its oceanization.

Data Availability Statement

The main results derived from the 3D geological model presented in Figure 8 (sedimentary cover thickness, geometry of the intruded batholith causing the Pacific Margin Anomaly and depth of the Moho) are available for download at the DIGITAL.CSIC repository: http://hdl.handle.net/10261/304015.

Acknowledgments
We thank Dr. Graeme Eagles and another anonymous reviewer who helped improving the manuscript with their very constructive comments. We would like to thank also to Professor Jonathan Aitchison and Dr. Augusto Rapalini the for their editorial handling of the manuscript. This research was funded by the Spanish Ministry of Science, Innovation and Universities predoctoral Grant PRE2018-084612 linked to the coordinated project TASDRACC (CTM2017-89711-C2-1P and CTM2017-89711-C2-2P), cofounded by the European Union through FEDER funds. The WDMAM compilation of magnetic anomalies used in this work is available at: http://wdmam.org/. Free-air gravity data database can be found at: https://topex.ucsd.edu/. The seismicity data is available at the USGS earthquake catalog: https://earthquake.usgs.gov/. This research used data provided by the Scientific Committee on Antarctic Research (SCAR) Seismic Data Library System (SDLS) accessible on the website: http://sdls.ogs.trieste.it/. Finally, the GEBCO bathymetric data is provided at: https://download.gebco.net/.

References

Alvey, A., Gaina, C., Kusznir, N. J., & Torsvik, T. H. (2008). Integrated crustal thickness mapping and plate reconstructions for the high Arctic. *Earth and Planetary Science Letters*, *274*(3–4), 310–321. https://doi.org/10.1016/j.epsl.2008.07.036

Amenábar, C. R., Montes, M., Nozal, F., & Santillana, S. (2020). Dinoflagellate cysts of the la Meseta Formation (middle to late Eocene), Antarctic Peninsula: Implications for biostratigraphy, palaeoceanography and palaeoenvironment. *Geological Magazine*, *157*(3), 351–366. https://doi.org/10.1017/S0016756819000591

Arndt, J. E., Schenke, H. W., Jakobsson, M., Nitsche, F. O., Buys, G., Goleby, B., et al. (2013). The International Bathymetric Chart of the Southern Ocean (IBCSO) Version 1.0—A new bathymetric compilation covering circum-Antarctic waters. *Geophysical Research Letters*, *40*(12), 3111–3117. https://doi.org/10.1002/grl.50413

Barber, P. L., Barker, P. F., & Pankhurst, R. J. (1991). Dredged rocks from Powell Basin and the South Orkney Microcontinent. In *International Symposium on Antarctic Earth Sciences* (Vol. 5, pp. 361–367).

Barker, P. E., Kennett, J. P., & Participating Scientist. (1988). In *Procedings of the Ocean Drilling Program*, *Initial Reports* (Vol. 113). Ocean Drilling Program. https://doi.org/10.2973/odp.proc.ir.113.1988

Barker, P. F., & Burrell, J. (1977). The opening of Drake Passage. *Marine Geology*, *25*(1–3), 15–34. https://doi.org/10.1016/0025-3227(77)90045-7

Barker, P. F., & Dalziel, I. W. (1983). Progress in Geodynamics in the Scotia Arc Region. *Geodynamics of the Eastern Pacific Region, Caribbean and Scotia Arcs* (Vol. *9*, pp. 137–170). https://doi.org/10.1029/gd009p0137

Barker, P. F., Dalziel, I. W. D., & Storey, B. C. (1991). Tectonic development of the Scotia arc region. *The Geology of Antarctica* (pp. 215–248).

Barker, P. F., & Griffiths, D. H. (1972). A discussion on volcanism and the structure of the Earth-The evolution of the Scotia Ridge and Scotia Sea. *Philosophical Transactions of the Royal Society of London - Series A: Mathematical and Physical Sciences*, *271*(1213), 151–183. https://doi.org/10.1098/rsta.1972.0005

Bijl, P. K., Sluijs, A., & Brinkhuis, H. (2013). A magneto- and chemostratigraphically calibrated dinoflagellate cyst zonation of the early Palaeogene South Pacific Ocean. *Earth-Science Reviews*, *124*, 1–31. https://doi.org/10.1016/j.earscirev.2013.04.010

Bohoyo, F. (2004). *Fragmentación continental y desarrollo de cuencas oceánicas en el sector meridional del Arco de Scotia, Antártida* (Doctoral Thesis). University of Granada.

Bohoyo, F., Galindo-Zaldívar, J., Jabaloy, A., Maldonado, A., Rodríguez-Fernández, J., Schreider, A., & Suriñach, E. (2007). Extensional deformation and development of deep basins associated with the sinistral transcurrent fault zone of the Scotia-Antarctic plate boundary. *Geological Society, London, Special Publications*, *290*(1), 203–217. https://doi.org/10.1144/SP290.6

Bohoyo, F., Galindo-Zaldívar, J., Maldonado, A., Schreider, A. A., & Suriñach, E. (2002). Basin development subsequent to ridge-trench collision: The Jane Basin, Antarctica. *Marine Geophysical Research*, *23*(5/6), 413–421. https://doi.org/10.1023/B:MARI.0000018194.18098.0d

Busetti, M., Zanolla, M., & Marchetti, A. (2000). Geological structure of the South Orkney Microcontinent. *Terra Antartica*, *8*(2), 1–8.

Calcagno, P., Chilès, J. P., Courrioux, G., & Guillen, A. (2008). Geological modelling from field data and geological knowledge. Part I. Modelling method coupling 3D potential-field interpolation and geological rules. *Physics of the Earth and Planetary Interiors*, *171*(1–4), 147–157. https://doi.org/10.1016/j.pepi.2008.06.013

Catalán, M., Martos, Y. M., Galindo-Zaldivar, J., Perez, L. F., & Bohoyo, F. (2020). Unveiling Powell Basin's tectonic domains and understanding its abnormal magnetic anomaly signature. Is heat the key? *Frontiers in Earth Science*, *8*, 580675. https://doi.org/10.3389/feart.2020.580675

Chen, L. (2014). Stretching factor estimation for the long-duration and multi-stage continental extensional tectonics: Application to the Baiyun Sag in the northern margin of the South China Sea. *Tectonophysics*, *611*, 167–180. https://doi.org/10.1016/j.tecto.2013.11.026

Civile, D., Lodolo, E., Vuan, A., & Loreto, M. F. (2012). Tectonics of the Scotia-Antarctica plate boundary constrained from seismic and seismological data. *Tectonophysics*, *550–553*, 17–34. https://doi.org/10.1016/j.tecto.2012.05.002

Dalziel, I. W. (1984). *Tectonic evolution of a forearc terrane, southern Scotia Ridge, Antarctica* (Vol. 200). Geological Society of America. https://doi.org/10.1029/eo067i007p00080

Dalziel, I. W. D., Lawver, L. A., Pearce, J. A., Barker, P. F., Hastie, A. R., Barfod, D. N., et al. (2013). A potential barrier to deep Antarctic circumpolar flow until the late Miocene? *Geology*, *41*(9), 947–950. https://doi.org/10.1130/G34352.1

Dentith, M., & Mudge, S. T. (2014). *Geophysics for the mineral exploration geoscientist*. Cambridge University Press. https://doi.org/10.1017/cbo9781139024358

Dickens, W. A., Graham, A. G. C., Smith, J. A., Dowdeswell, J. A., Larter, R. D., Hillenbrand, C. D., et al. (2014). A new bathymetric compilation for the South Orkney Islands region, Antarctic Peninsula (49°–39°W to 64°–59°S): Insights into the glacial development of the continental shelf. *Geochemistry, Geophysics, Geosystems*, *15*(6), 2494–2514. https://doi.org/10.1002/2014GC005323

Doo, W. B., Hsu, S. K., Tsai, C. H., & Huang, Y. S. (2009). Using analytic signal to determine magnetization/density ratios of geological structures. *Geophysical Journal International*, *179*(1), 112–124. https://doi.org/10.1111/j.1365-246X.2009.04297.x

Eagles, G., & Eisermann, H. (2020). The Skytrain plate and tectonic evolution of southwest Gondwana since Jurassic times. *Scientific Reports*, *10*(1), 1–17. https://doi.org/10.1038/s41598-020-77070-6

Eagles, G., & Jokat, W. (2014). Tectonic reconstructions for paleobathymetry in Drake Passage. *Tectonophysics*, *611*, 28–50. https://doi.org/10.1016/j.tecto.2013.11.021

Eagles, G., & Livermore, R. A. (2002). Opening history of Powell Basin, Antarctic Peninsula. *Marine Geology*, *185*(3–4), 195–205. https://doi.org/10.1016/S0025-3227(02)00191-3

Galindo-Zaldívar, J., Bohoyo, F., Maldonado, A., Schreider, A., Suriñach, E., & Vázquez, J. T. (2006). Propagating rift during the opening of a small oceanic basin: The Protector Basin (Scotia Arc, Antarctica). *Earth and Planetary Science Letters*, *241*(3–4), 398–412. https://doi.org/10.1016/j.epsl.2005.11.056

Garrett, S. W. (1990). Interpretation of reconnaissance gravity and aeromagnetic surveys of the Antarctic Peninsula. *Journal of Geophysical Research*, *95*(B5), 6759–6777. https://doi.org/10.1029/JB095iB05p06759

Garrett, S. W., Renner, R. G. B., Jones, J. A., & McGibbon, K. J. (1986). Continental magnetic anomalies and the evolution of the Scotia Arc. *Earth and Planetary Science Letters*, *81*(2–3), 273–281. https://doi.org/10.1016/0012-821X(87)90163-4

Garrett, S. W., & Storey, B. C. (1987). Lithospheric extension on the Antarctic Peninsula during Cenozoic subduction. *Geological Society, London, Special Publications*, *28*(1), 419–431. https://doi.org/10.1144/GSL.SP.1987.028.01.26

GEBCO Compilation Group. (2020). GEBCO 2020 Gridded Bathymetry data[Dataset]. GEBCO. https://doi.org/10.5285/a29c5465-b138-234d-e053-6c86abc040b9

Gemperle, M., Conrad, G., Sargen, M. Y., & Starr, S. (1991). Geosoft GM-SYS v. 1.8 [Software]. Northwest Geophysical Associates, Inc, 65.

Harrington, P. K., Barker, P. F., & Griffiths, D. H. (1972). Crustal structure of the South Orkney Islands area from seismic refraction and magnetic measurements. In *Paper presented at Symposium on Antarctic Geology and Solid Earth Geophysics in August 1970, Oslo*.

Hsu, S. K., Coppens, D., & Shyu, C. T. (1998). Depth to magnetic source using the generalized analytic signal. *Geophysics*, *63*(6), 1947–1957. https://doi.org/10.1190/1.1444488

Kavoun, M., & Vinnikovskaya, O. (1994). Seismic stratigraphy and tectonics of the northwestern Weddell Sea (Antarctica) inferred from marine geophysical surveys. *Tectonophysics*, *240*(1–4), 299–341. https://doi.org/10.1016/0040-1951(94)90277-1

King, E. C., & Barker, P. F. (1988). The margins of the South Orkney Microcontinent. *Journal of the Geological Society*, *145*(2), 317–331. https://doi.org/10.1144/gsjgs.145.2.0317

King, E. C., Leitchenkov, G., Galindo-Zaldivar, J., Maldonado, A., & Lodolo, E. (1997). Crustal structure and sedimentation in Powell Basin. *Geology and Seismic Stratigraphy of the Antarctic Margin*, *2*(71), 75–93. https://doi.org/10.1029/ar071p0075

Kirby, S. H. (1983). Rheology of the lithosphere. *Reviews of Geophysics*, *21*(6), 1458–1487. https://doi.org/10.1029/RG021i006p01458

Lajaunie, C., Courrioux, G., & Manuel, L. (1997). Foliation fields and 3D cartography in geology: Principles of a method based on potential interpolation. *Mathematical Geology*, *29*(4), 571–584. https://doi.org/10.1007/bf02775087

Lawver, L. A., Sclater, J. G., & Meinke, L. (1985). Mesozoic and Cenozoic reconstructions of the South Atlantic. *Tectonophysics*, *114*(1–4), 233–254. https://doi.org/10.1016/0040-1951(85)90015-0

Lesur, V., Hamoudi, M., Choi, Y., Dyment, J., & Thébault, E. (2016). Building the second version of the World Digital Magnetic Anomaly Map (WDMAM). *Earth, Planets and Space*, *68*(1), 1–13. https://doi.org/10.1186/s40623-016-0404-6

Livermore, R., Hillenbrand, C. D., Meredith, M., & Eagles, G. (2007). Drake Passage and Cenozoic climate: An open and shut case? *Geochemistry, Geophysics, Geosystems*, *8*(1), Q01005. https://doi.org/10.1029/2005GC001224

Livermore, R., Nankivell, A., Eagles, G., & Morris, P. (2005). Paleogene opening of Drake Passage. *Earth and Planetary Science Letters*, *236*(1–2), 459–470. https://doi.org/10.1016/j.epsl.2005.03.027

López-Quirós, A., Escutia, C., Etourneau, J., Rodríguez-Tovar, F. J., Roignant, S., Lobo, F. J., et al. (2021). Eocene-Oligocene paleoenvironmental changes in the South Orkney Microcontinent (Antarctica) linked to the opening of Powell Basin. *Global and Planetary Change*, *204*, 103581. https://doi.org/10.1016/j.gloplacha.2021.103581

Maestro, A., López-Martínez, J., & Bohoyo, F. (2013). Mesozoic to recent evolution of intraplate stress fields under multiple remote stresses: The case of Signy Island (South Orkney Microcontinent, Antarctica). *Geological Society, London, Special Publications*, *381*(1), 45–65. https://doi.org/10.1144/SP381.4

Maldonado, A., Bohoyo, F., Galindo-Zaldívar, J., Hernández-Molina, F. J., Lobo, F. J., Lodolo, E., et al. (2014). A model of oceanic development by ridge jumping: Opening of the Scotia Sea. *Global and Planetary Change*, *123*, 152–173. https://doi.org/10.1016/j.gloplacha.2014.06.010

Mallet, J. L. (2002). *Geomodeling*. Oxford University Press.

Martos, Y. M., Catalán, M., Galindo-Zaldívar, J., Maldonado, A., & Bohoyo, F. (2014). Insights about the structure and evolution of the Scotia Arc from a new magnetic data compilation. *Global and Planetary Change*, *123*, 239–248. https://doi.org/10.1016/j.gloplacha.2014.07.022

McKenzie, D. (1978). Some remarks on the development of sedimentary basins. *Earth and Planetary Science Letters*, *40*(1), 25–32. https://doi.org/10.1016/0012-821X(78)90071-7

Montes, M., Beamud, E., Nozal, F., & Santillana, S. N. (2019). Late Maastrichtian-Paleocene chronostratigraphy from Seymour Island (James Ross Basin, Antarctic Peninsula). Eustatic controls on sedimentation. *Advances in Polar Science*, *30*(2), 1–12. https://doi.org/10.13679/j.advps.2019.2.00

Northwest Geophysical Associates. (2004). *GM-SYS gravity/magnetic modeling software. User's guide, Version 4.9* (p. 101). Northwest Geophysical Associates.

Ranalli, G., & Murphy, D. C. (1987). Rheological stratification of the lithosphere. *Tectonophysics*, *132*(4), 281–295. https://doi.org/10.1016/0040-1951(87)90348-9

Reguzzoni, M., & Sampietro, D. (2015). GEMMA: An Earth crustal model based on GOCE satellite data. *International Journal of Applied Earth Observations and Geoinformation*, *35*, 31–43. https://doi.org/10.1016/j.jag.2014.04.002

Renner, R. G. B., Dikstra, B. J., & Martin, J. L. (1982). Aeromagnetic Surveys over the Antarctic Peninsula. In *Paper presented at Symposium on Antarctic Geology and Geophysics in 1977, Madison, Wisconsin*.

Riley, T. R., Carter, A., Burton-Johnson, A., Leat, P. T., Hogan, K. A., & Bown, P. R. (2022). Crustal block origins of the South Scotia Ridge. *Terra Nova*, *34*(6), 495–502. https://doi.org/10.1111/ter.12613

Rodriguez-Fernandez, J., Balanya, J. C., Galindo-Zaldivar, J., & Maldonado, A. (1997). Tectonic evolution of a restricted ocean basin: The Powell Basin (Northeastern Antarctic Peninsula). *Geodinamica Acta*, *10*(4), 159–174. https://doi.org/10.1080/09853111.1997.11105300

Roest, W. R., & Pilkington, M. (1993). Identifying remanent magnetization effects in magnetic data. *Geophysics*, *58*(5), 653–659. https://doi.org/10.1190/1.1443449

Roest, W. R., Verhoef, J., & Pilkington, M. (1992). Magnetic interpretation using the 3-D analytic signal. *Geophysics*, *57*(1), 116–125. https://doi.org/10.1190/1.1443174

Sandwell, D. T., Müller, R. D., Smith, W. H. F., Garcia, E., & Francis, R. (2014). New global marine gravity model from Cryo-Sat-2 and Jason-1 reveals buried tectonic structure. *Science*, *346*(6205), 65–67. https://doi.org/10.1126/science.1258213

Schreider, A. A., Sazhneva, A., Kluyev, M. S., Brekhovskikh, A. L., Bohoyo, F., Galindo-Zaldivar, J., et al. (2022). Kinematic model of the development of the bottom of the Powell Basin (Weddell Sea). *Processes in GeoMedia*, *5*, 197–207. https://doi.org/10.1007/978-3-030-85851-3_22

Simpson, R. W., Jachens, R. C., & Blakely, R. J. (1983). *AIRYROOT; a FORTRAN program for calculating the gravitational attraction of an Airy isostatic root out to 166.7 km (No. 83-883)*. US Geological Survey. https://doi.org/10.3133/ofr83883

Smith, W., & Sandwell, D. (1997). Global sea floor topography from satellite altimetry and sparse shipboard bathymetry. *Science*, *277*(5334), 1956–1961. https://doi.org/10.1126/science.277.5334.1956

Suriñach, E., Galindo-Zaldivar, J., Maldonado, A., & Livermore, R. (1997). Large amplitude magnetic anomalies in the northern sector of the Powell Basin, NE Antarctic Peninsula. *Marine Geophysical Research*, *19*(1), 65–80. https://doi.org/10.1023/A:1004240931967

Telford, W. M., Geldart, L. P., & Sheriff, R. E. (1990). *Applied geophysics*. Cambridge university press.

Thompson, N., Salzmann, U., López-Quirós, A., Bijl, P. K., Hoem, F. S., Etourneau, J., et al. (2022). Vegetation change across the Drake Passage region linked to late Eocene cooling and glacial disturbance after the Eocene-Oligocene transition. *Climate of the Past*, *18*(2), 209–232. https://doi.org/10.5194/cp-18-209-2022

Trouw, R. A. J., Passchier, C. W., Simões, L. S. A., Andreis, R. R., & Valeriano, C. M. (1997). Mesozoic tectonic evolution of the South Orkney Microcontinent, Scotia Arc, Antarctica. *Geological Magazine*, *134*(3), 383–401. https://doi.org/10.1017/S0016756897007036

van de Lagemaat, S. H. A., Swart, M. L. A., Vaes, B., Kosters, M. E., Boschman, L. M., Burton-Johnson, A., et al. (2021). Subduction initiation in the Scotia Sea region and opening of the Drake Passage: When and why? *Earth-Science Reviews*, *215*, 103551. https://doi.org/10.1016/j.earscirev.2021.103551

Vaughan, A. P. M., Wareham, C. D., Johnson, A. C., & Kelley, S. P. (1998). A lower Cretaceous, syn-extensional magmatic source for a linear belt of positive magnetic anomalies: The Pacific Margin Anomaly (PMA), western Palmer Land, Antarctica. *Earth and Planetary Science Letters*, *158*(3–4), 143–155. https://doi.org/10.1016/S0012-821X(98)00054-5

Wu, Q., Xu, H., & Zou, X. (2005). An effective method for 3D geological modeling with multi-source data integration. *Computers & Geosciences*, *31*(1), 35–43. https://doi.org/10.1016/j.cageo.2004.09.005

Zhang, Y. F., Sun, Z., Zhou, D., Guo, X. W., Shi, X., Wu, X. J., & Pang, X. (2008). Stretching characteristics and its dynamic significance of the northern continental margin of South China Sea. *Science in China - Series D: Earth Sciences*, *51*(3), 422–430. https://doi.org/10.1007/s11430-008-0019-2